Energy harvesting and storage for stand-alone microsystems

10

R.H. Gounella[1], *Y.A.O. Assagra*[1], *L.M. Gonçalves*[2] *and J.P. Carmo*[1]
[1]Department of Electrical Engineering (SEL), University of São Paulo (USP), São Carlos, Brazil, [2]Department of Industrial Electronics (DEI), University of Minho (UMinho), Guimarães, Portugal

Chapter Outline

10.1 Introduction

It is not new to anyone that since the last decade, wireless communication microsystems (MSTs) with a high density of nodes and simple protocols have emerged for low data rate distributed sensor network applications such as those in home automation [1,2] and industrial control [3,4]. In this context, the grown interest to implement the paradigm of using independent operation, management, and maintenance in wireless sensors networks, pushed the requirements in WSN nodes to present even more low-power consumption [5,6]. Additionally, there is also an increasing interest in ubiquitous electronic devices in the everyday life [7,8]. Also, the complexity and the requirements of these devices do not know limits. The use of batteries cannot be enough to ensure an uninterruptible working cycle due to its limited capacity. For example, the capacity of commercial class AA batteries (the most suitable for powering stand-alone microsystems for ready deployment) is limited to 3000 mAh [9]. This is of major importance, especially in the operation of stand-alone microsystems to be supplied by the energy harvested from the surrounding environment. Thus, the association of such devices with the use of some kind of energy recovering system can reveal an interesting approach [10]. Energy scavengers are currently emerging for a number of applications from biomedical to automotive [11,12]. The three most important energy sources of interest for use in remote micro/nanosystems are thermoelectric (from thermal gradients), piezoelectric (from mechanical vibrations), and photovoltaic (from solar light). The piezoelectric harvesting systems are widely

Emerging Trends in Energy Storage Systems and Industrial Applications. DOI: https://doi.org/10.1016/B978-0-323-90521-3.00002-8

settled and validated, however, direct thermal-to-electric energy conversion without moving mechanical parts is attractive for a wide range of applications because it provides compact and distributed power, quiet operation, and is usually environmentally friendly. Thus, it is not strange the fact worldwide efforts are being undertaken to expand the technology of thermoelectric devices into the field of microsystems technologies and more covered in this chapter than other harvesting techniques. Today, almost all of these platforms are designed to run on batteries that not only have a very limited lifetime but are also in many areas a cost-prohibitive solution. An attractive alternative is powering the sensors with energy harvested from the environment. Thus, a solution for energy generation through energy harvesting by taking advantage of temperature differences must be found. Since many wireless sensors are powered on a peak basis (e.g., the transmission of data needs much more current than standby or receiving mode) and the environmental condition could not always be present, the energy can be stored in a rechargeable thin-film battery of Li-ion type (integrated into the system). Ultra-low-power electronics perform DC—DC rectification with a variable conversion factor and recharge the battery under optimal conditions. All of these issues are discussed further in this review.

10.2 Energy harvesting systems

Energy harvesters for stand-alone microsystems are currently emerging for a number of applications from medicine to automotive. Typically, one can distinguish between two types of energy scavengers, for example, macro-energy scavengers that are typically in the cm^3 range, whereas the micro-energy scavengers that are typically in the mm^3 range and manufactured using micromachining techniques. Micro-energy harvesters are small electromechanical devices that harvest ambient energy and convert it into electricity [12]. Energy harvesters can collect different types of energies. The solar energy can be collected and stored by means of photovoltaic solar cells with a charge-integrating capacitor for periods of darkness [13], mechanical energy can be collected with piezoelectric or electrostatic converters [14], electromagnetic energy can be collected through radio frequency resonators [15], and finally, thermal energy can be collected with thermoelectric generators [16]. The majority of the micro-energy harvesters are still in the research and development phase. However, thermoelectrics was the first one to appear in the market [12]. This was due to the easiness to fabricate these devices with solid-state technology and because their working principle is based on a well-established physical theory. Table 10.1 resumes the majority of features that characterizes each type of energy harvesting presented in this review. Next, in the further sections, a few energy harvesting types are presented.

10.2.1 Thermoelectric

In 1821, Seebeck observed that the needle of a magnet is deflected in the presence of dissimilar metals that are connected (electrically in series and thermally in

Table 10.1 The list with the majority of features that characterizes each type of energy harvesting is presented in this review.

Energy sources in the environment	Main challenge(s)	Magnitude for the typical impedance	Magnitude for the typical voltage	Magnitude for the typical output power
Light (solar type)	Conformal with small surface areas, wide range for the input voltage	Varying with the light intensity, from a few kΩ to dozens of kΩ	DC: from 0.5 V up to 5 V, depending on the number of PC cells	Outdoors: from a few μW up to a few mW Indoors: from a few hundredths of mW up to a few mW
Mechanical vibration (piezoelectric type)	Narrow-band and high selective: pose problems of frequency variability in mechanical vibrations	Almost constant: from a few dozens Ω up to a few hundreds of Ω	AC: few dozens of V	Ranging from a few μW up to a few dozens of mW
Thermoelectric	Small thermal gradients, efficient heat skinking	Almost constant: from few Ω up to a few hundreds of Ω	DC: from both few dozens of mW up to V	Gradient of 20°C: from a few hundreds of μW up to a few dozens of mW

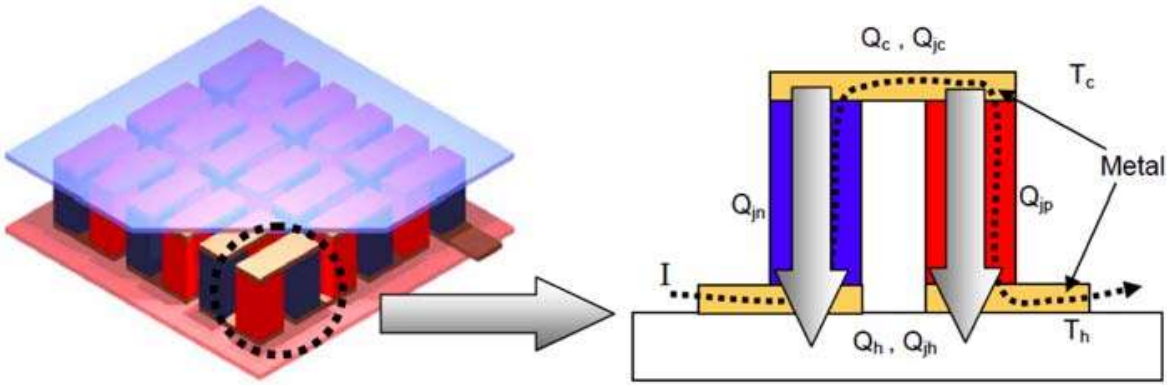

Figure 10.1 An artist's impression of a typical thermoelectric generator and a zoomed view of a thermoelectric pair (e.g., a thermoleg).

parallel) and exposed to a temperature gradient [16]. The effect he observed is the basis for thermoelectric power generation. Fig. 10.1 shows the basic cell of a typical thermoelectric microgenerator, which is composed of two thermoelectric columns (n-type and p-type). As shown in Fig. 10.1, if the junctions at the bottom are heated and those at the top are cooled (producing a temperature differential), electron/hole pairs will be created at the hot end and absorb heat in the process. The pairs recombine and reject heat at the cold ends. A voltage potential, the Seebeck voltage, which drives the hole/electron flow, is created by the temperature difference between the hot and cold ends of the thermoelectric elements. The net voltage appears across the bottom of the thermoelectric element legs.

The physics of these energy converters are widely known and dominated, imposing the research effort in the discovery and research of new materials and structures to make the process of current extraction from thermal gradients the most efficient as possible. This implies obtaining materials (both in the bulk [17], nanostructured [18], and/or superlattice [19] forms) that simultaneously are good electric conductors to minimize heat losses by the Joule effect, poor thermal conductors to retain the most heat possible at the site of the junction and at the same time presenting a maximum Seebeck effect, to produce the required voltage [20]. The performance of thermoelectric devices depends on the figure of merit ZT of the material [19,21] and is a dimensionless quantity, which is given by:

$$ZT = \frac{\alpha^2}{\rho\lambda} T \tag{10.1}$$

where α [V K^{-1}] is the Seebeck coefficient, ρ [Ω m] the electrical resistivity (e.g., the inverse of the electrical conductivity S [S m^{-1}]), λ [W m^{-1} K^{-1}] the thermal conductivity and T [K] the temperature. Another performance factor is more appropriate on thermoelectric devices, for example, the power-factor PF [W K^{-2} m^{-1}], expressed in terms of:

$$PF = \frac{\alpha^2}{\rho} \left[\mathrm{W\ K^{-2} m^{-1}}\right] \tag{10.2}$$

Analyzing the two equations above, it is desirable to select a material or group of materials that maximize both the *ZT* and *PF*, Unfortunately, the three physical quantitiesα, ρ and λ trade between them, meaning that their mutual interdependencies must be taken when a simultaneous optimization of these properties is desired. The simple fact the electrons carry unwanted heat and electric charge (traduced as electrical current) will decrease the Seebeck effect while the electrical conductivity increases. For bulk materials at both macro- and micro-scales, the highest performance is obtained in the presence of heavily doped semiconductors, such as bismuth telluride [22] or silicon-germanium [23]. For the case of semiconductors, the most desirable situation is when the base materials are both *n*- and *p*-doped to apply the same material system on both sides of the junctions [16]. Also, to be used in microsystems, a thermoelectric generator must be small in size, light in weight, and possibly have fabrication compatibility with the microsystem elements. Thin-film generators are the most suited for microsystems applications since they give the advantage of obtaining modules with minimum size and weight [20].

A lot of new developments about thermoelectric converters for energy harvesting can be found in the literature. This review tries to focus on the most updated and the ones with the most potential for a technological breakthrough, as well as in the case of authors' work. The work developed by Yang et al. [23] can be considered unique in the fact it presents a thermoelectric converter directly fabricated on top of a CMOS device. Thanks to the used material based on polysilicon (in fact, as reproduced in Fig. 10.2A, using the polysilicon-1 layer serves as p-type thermoleg, and the polysilicon-2 layer serves as n-type thermoleg, both represented respectively by red and green strips) [23]. In order to force the heat flow to take in the lateral region, a cavity was etched below the thermoelectric pairs, in a way to form a

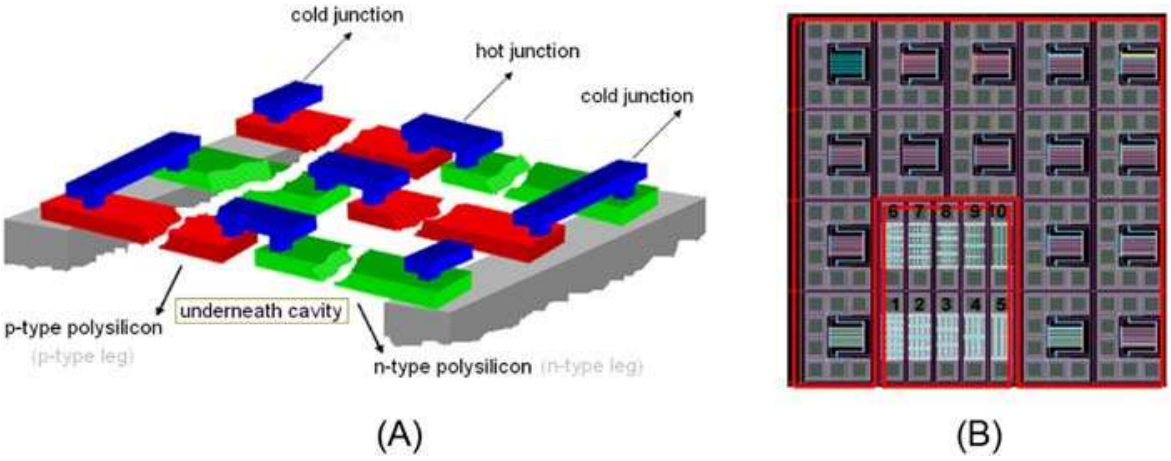

Figure 10.2 For the work developed by Yang et al.: (A) an artist impression showing the schematic diagram of a micro thermoelectric converter (working as thermogenerator) with thermal isolation cavity on the bottom of thermoelectric pairs in polysilicon; and (B) a photo of a microdevice prototype (with a square area of 4 mm^2) containing 10 thermoelectric converters (red square on bottom) and test structures (the remaining area delimited by red lines distributed around the perimeter) [23].
Source: Reproduced with the previous authorization of the publisher (*Elsevier*).

membrane with minimum thermal conductivity. The hot side of the device is the upper plane in the region above the thermoelectric pairs in silicon, while the cold side is the plane located below the cavity. The underneath cavity ensures thermal isolation to prevent heat loss, maintain the temperature gradient and increase the efficiency by improving the output power [23]. Their simulations were applied on a thermoelectric junction (e.g., thermocouple) with optimal dimensions of $71 \times 4 \times 0.275/0.18$ μm (defined as length × width × thickness for p-/n-thermolegs) showed a maximum power factor of 0.047 $\mu W\ cm^{-2}\ K^{-2}$ and a voltage factor of 2.788 $V\ cm^{-2}\ K^{-1}$. They also observed a power factor of 0.042 $\mu W\ cm^{-2}\ K^{-2}$ from a thermocouple (measuring 60×4 μm) within a functional prototype of a microdevice fabricated in the TSMC 0.35 μm CMOS process with 2 layers of polysilicon and 4 layers of metal [23].

The field of human body applications experiments a grown in the demand in last years, ranging from the acquisition of physiological information of several kinds [24–30]. This field is also known as Body-Area Networks or BAN [31–33]. Thus, it is also not strange the growth of these applications using energy harvesting [31,34]. The authors of the work found in [34] made an optimized design of a full-fledged wearable miniaturized thermoelectric specifically for use in human body applications. As illustrated in Fig. 10.3A, such a converter has a shape with a rim structure. This structure was obtained by surface micromachining applied to the polycrystalline silicon–germanium (poly-SiGe). The photos of these converters and a few zoomed views can be observed in Fig. 10.3B. In terms of fabrication details, each thermoelectric converter can contain 2350 or 4700 thermocouples, thermally connected in parallel and electrically in series. In their experimentations, the authors made a flip-chip bond of the converter into an electronic microdevice coated with a thin-layer of BCB. Such a configuration demonstrated the ability to deliver an open-circuit voltage of 12.5 $V\ K^{-1}\ cm^{-2}$ and output power of 0.026 $\mu W\ cm^{-2}\ K^{-2}$ on a matched external load [34]. The experimental tests also showed that under real field conditions, for example, being worn on the human body, this thermoelectric generator can deliver an open-circuit output voltage of ≈ 0.15 V and output power of ≈ 0.3 nW when supplying a matched load.

An outstanding application of thermoelectric converters on BAN can be found in [31], where the authors designed and fabricated readout circuits for the acquisition of biopotential signals. These circuits were optimized for low-power and high-performance, to allow stand-alone applications outside clinical environments and without the need for any kind of intervention from health professionals. Fig. 10.4A shows the photo of a functional prototype of a wireless EEG acquisition system with eight channels, occupying only 1 cm^3 [31]. In Fig. 10.4B, it is possible to observe a thermoelectric generator (composed of 10 sections, each measuring 1.6×4 cm) to supply the previous EEG acquisition system. It is interesting to observe the conformity of the generator with the shape of the subject's forehead [31]. According to the Ref. [18] of their work, the thermoelectric generator was designed to work at room temperatures up to 26°C. Additionally, it is claimed the ability to deliver a power of about 2 mW (e.g., a power density of 30 $\mu W\ cm^2$) for

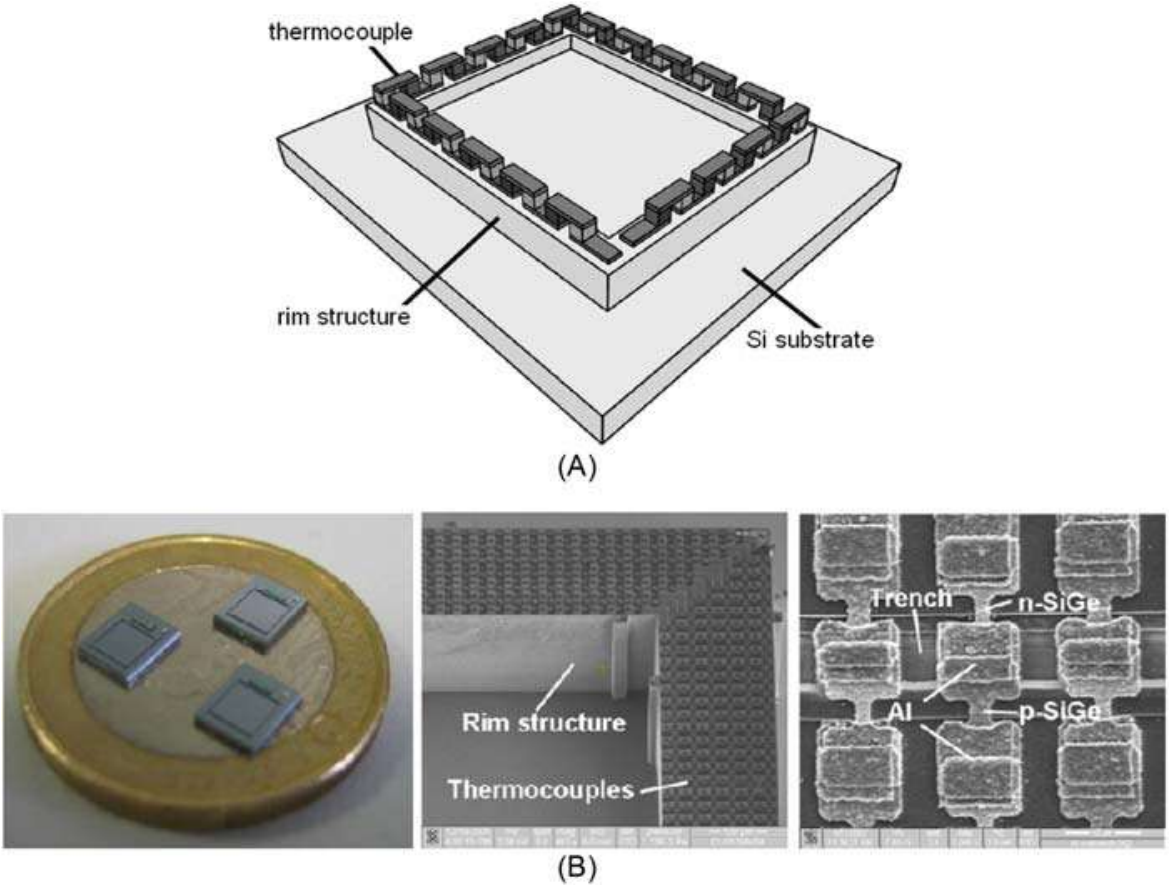

Figure 10.3 For the work developed by Wang et al.: (A) an artist impression showing the schematic of their thermoelectric converter, where it can be observed the several micromachined thermocouples after being fabricated on top of a rim structure with a height of 250 μm. (B) Progressively zoomed photos (from left to right) of a few functional prototypes of micromachined thermoelectric pairs; the middle and right photos only can be observed through SEM microscopy, where the middle one shows the rim structure and thermocouples; the photo on right shows a more deep close-up view of few micromachined thermocouples [34].
Source: Reproduced with the previous authorization of the publisher (Elsevier).

a room temperature of 23°C. This power is more than enough to supply the EEG acquisition system, whose power consumption is only 0.8 mW.

Thermoelectric converters based on bismuth tellurides [35] and both bismuth [36]/antimony [37] tellurides allow the fabrication of converters with high figures-of-merit *ZT* at room temperatures (e.g., 300K). In the context of this review, a high value of *ZT* is defined as one to be close to unity [19]. Unfortunately, this class of materials is not compatible with silicon, thus, requiring back-end techniques for their integration with microdevices based on silicon (e.g., CMOS technology). Despite this drawback, there are still excellent works of thermoelectric converters for energy harvesting using tellurides. The energy converter developed by Takashiri et al. [35] is a classical work focused on this class of materials and it was fabricated using the flash evaporation method through thermoelectric generators fabricated by a flash evaporation method. The n- and p-type powders of $Bi_{2.0}Te_{2.7}Se_{0.3}$ and

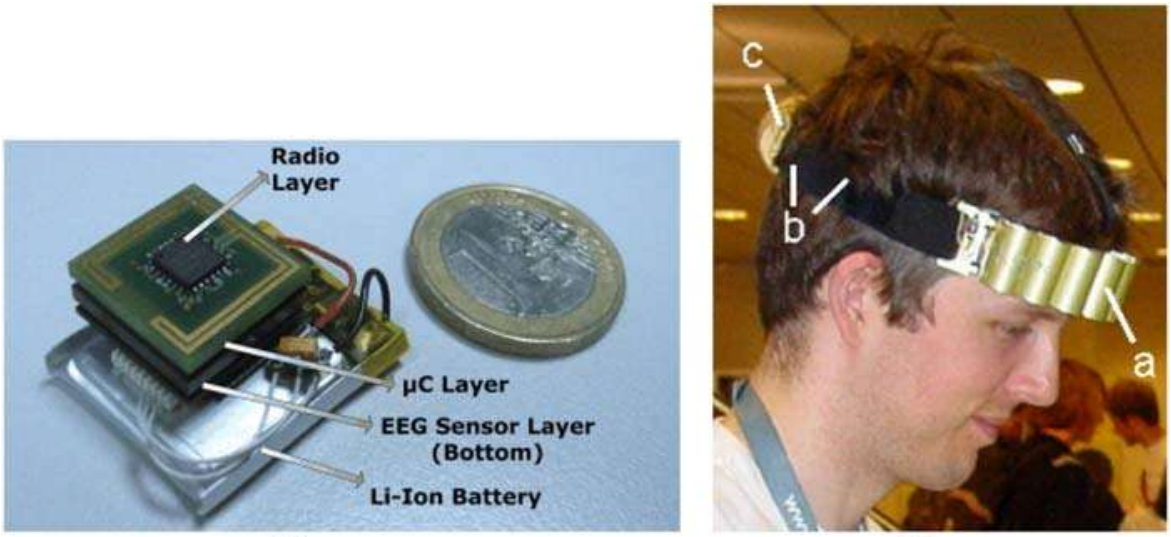

Figure 10.4 For the work developed by Yazicioglu et al.: (A) a photo of a data acquisition system with a capacity to acquire 8 EEG channels and (B) a photo of a thermoelectric converter placed in the forehead of a test subject to power the data acquisition system on left [31].
Source: Reproduced with the previous authorization of the publisher (Elsevier).

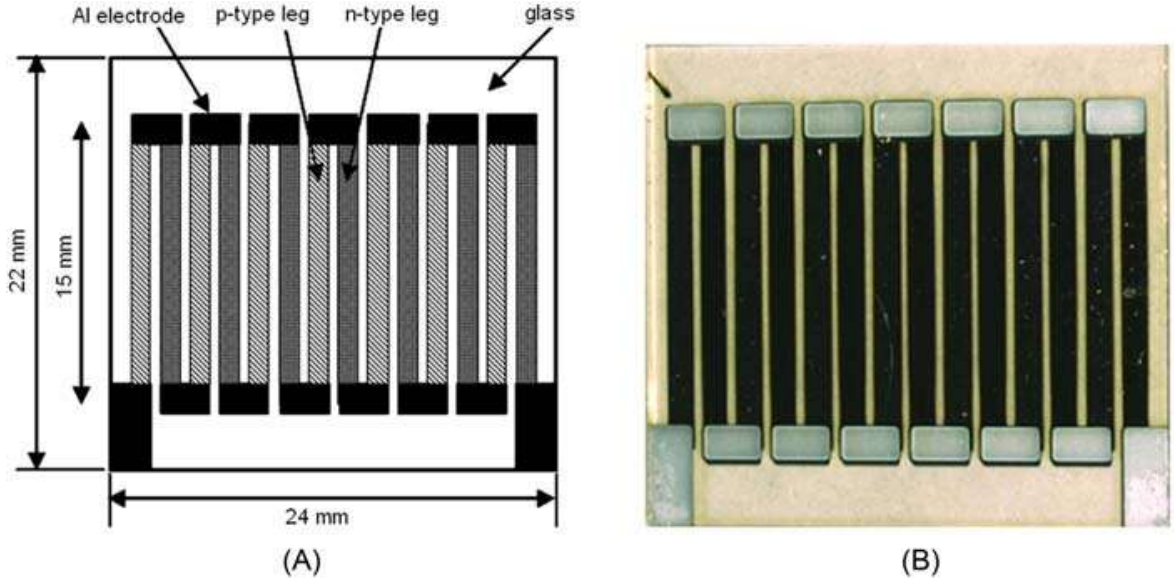

Figure 10.5 For the work developed by Takashiri et al.: (A) schematic and (B) photo of their functional prototype of thermoelectric converter [35].
Source: Reproduced with the previous authorization of the publisher (*Elsevier*).

$Bi_{0.4}Te_{3.0}Sb_{1.6}$ were respectively prepared for flash evaporation of thin films to form the thermoelectric legs (to make the thermoelectric pairs). As shown in Fig. 10.5 (schematic and photo), their thermoelectric converter is composed of seven pairs of thermolegs, electrically connected by electrodes made of aluminum [35]. Each leach measures $15 \times 1 \times 1$ mm (length × width × thickness) and their

physical arrangement and electrical connection result in a thermoelectric converter measuring 20 mm by 15 mm. After the fabrication of thermolegs, the thermoelectric characteristics of several functional prototypes were improved by submitting them to a hydrogen annealing at temperatures between 25°C and 250°C. For example, the functional prototype whose annealing temperature was of $T_a = 250$°C provided a maximum output voltage of 83.4 mV and an estimated power of 21 μV, when subjected to a temperature gradient of 30°C.

More works based on tellurides, more precisely planar thermoelectric generators based on bismuth and antimony tellurides can be found in [21] and [38]. Both converters were obtained using the deposition of thin-films. The difference relies on the fact that in the first case microsystems techniques were used (lithography and etching [21]), while the shadow mask technique was used in the second case [38]. Fig. 10.6A shows a magnified photo of a thermoelectric generator composed of eight pairs of n- and p-type elements [22]. A set of measurements were made for the Bi_2Te_3 and Sb_2Te_3 thin-films, resulting respectively in values of *ZT* at room temperatures of 0.97 and 0.56, and in power factors of 0.49 and 0.28 μW cm^{-2} K^{-2}. As it can be observed, the thermolegs were deposited on top of a polyimide foil with a thickness of 25 μm. The technique of shadow masks is simple and well used in thin-film depositions, where the distance precision is not critical. The n- and p-type deposited thin films are spaced apart between them by 500 μm. The contact area of the thermoelectric structures measures 1 mm^2, while the metal contacts made of aluminum occupy an area of 7 mm^2. A prototype proposed by Silva et al. [38] makes reminds the coiled-up thermoelectric generator fabricated by Weber et al. [39]. The prototype in Fig. 10.6B was obtained by sputtering thermolegs of bismuth and antimony on polyimide foils, whose geometry was based on the principle of the coiling-up to provide high values of voltages with smaller generator areas. This kind of geometries applied on a large strip of

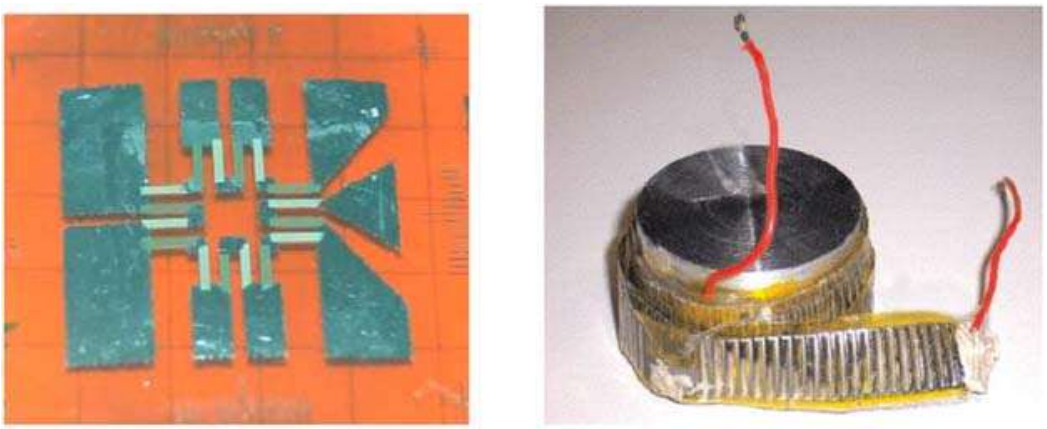

Figure 10.6 (A) Photo of a thermogenerator with eight pairs of n- and p-type elements, fabricated with bottom contacts [22]. (B) Photo of a coiled-up thermoelectric generator prototype [39].
Source: The photos on the left and right were reproduced with the previous authorization of the publisher (*Elsevier*).

polymer foil allows the fabrication of many thousands of thermocouples and the corresponding surround around the target structure where the temperature gradient is present [39].

A fascinating application using thermoelectric generators was validated by Wojtas et al. [40]. In strict terms, this application was already known on its fundaments, for example, by harvesting energy from the waste heat present in industrial processes [38] and vehicles [39]. The amazing difference relies on the involved scale, that is while the known approaches were implemented at the large size scale, the work of these authors [40] was implemented at the microscale. As illustrated in the photos Fig. 10.7, this application combines a microfluidic heat transfer system with a thermoelectric generator and is the first one of its kind reported in the literature. Their functional prototype was tested and characterized, considering two physical quantities: the measured thermal and hydrodynamic performance and the correspondent generated power [40].

The field of energy harvesting doesn't know limits when looking at the application of these systems on planes. In this context, a stand-alone sensorial node was designed and fabricated by Samson et al. [41] to operate on short-range flights. The work was validated on laboratory environment to deal with plane fuselage's temperatures in the range of −21.8°C to +20.4°C. The details about the choice of this temperature range as well as the specificities to deal with the several physical

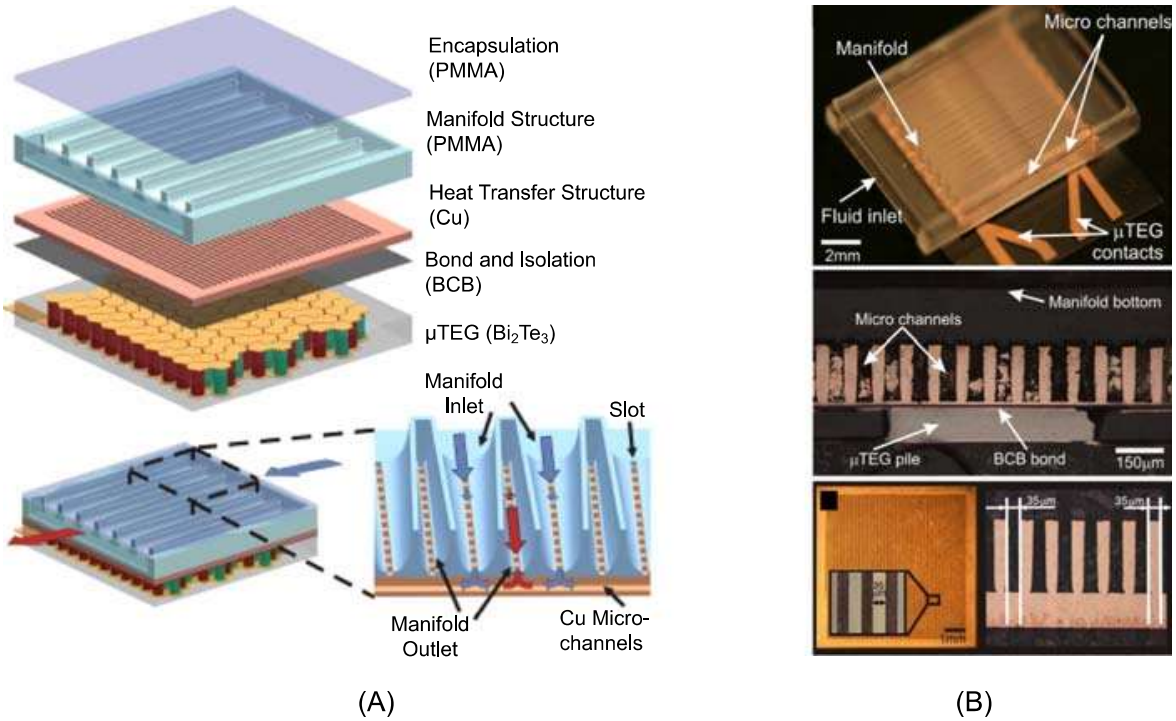

Figure 10.7 For the work developed by Wojtas et al.: (A) Exploded view illustrating the combination of a microfluidic heat transfer system with a thermoelectric generator, and the cross-section of the path where the hot fluid passes through; (B) photo of the functional prototype after being assembled (top), a cross-section of the path where the hot fluid passes through (middle) and top view (bottom) [40].
Source: Reproduced with the previous authorization of the publisher (*Elsevier*).

phenomena during [short-range] flights are fully detailed in their publication [41]. In this sequence of ideas and taking into account the temperature profile, the thermogenerator selection fell on a customized-made device from a well-known manufacturer for matching both the temperature range and profiles.

It must be noted that the voltage at the output of the thermogenerator is not constant and can drop below 1.5 V, thus, a power management chip is required to store the harvested energy and at the same time to make upconversion of the voltage to operate the sensorial node. In this work, a regulated voltage of 3.3 V is required. The tests in the laboratory environments have proven to be promised, thus, in the future is expected real-time tests in real-field operations [41]. Fig. 10.8 shows the block diagram and the respective photo of a stand-alone prototype mounted on an aircraft hull for future tests. The sensorial node is composed of a power management chip (implemented by a Texas Instruments MSP430 series microcontroller for intelligent management) and the sensorial node itself (composed of a crack wire sensor and by the Texas Instruments' CC2420 RF transceiver for the 2.4 GHz ISM band able to implement the standard IEEE 802.15.4 relative to the two lowest levels of the ZigBee's protocol). The experimental tests showed that the whole function prototype has a total power consumption of about 189 μW for an output voltage of 3.3 V [41].

New developments in materials with high *ZT*s (close to 1) are the only future way to follow to improve the characteristics of thermoelectric converters (both for energy harvesting and cold generation) and pave the way to increase the market and at the same time to decrease the costs (by providing high-volume production). It is undeniable the importance that was achieved up to now with telluride-based materials, both on bulk and microscale, but unfortunately, these materials are not compatible with the available technologies of microelectronics based on silicon [42]. Therefore, it is of major interest to develop materials compatible with silicon.

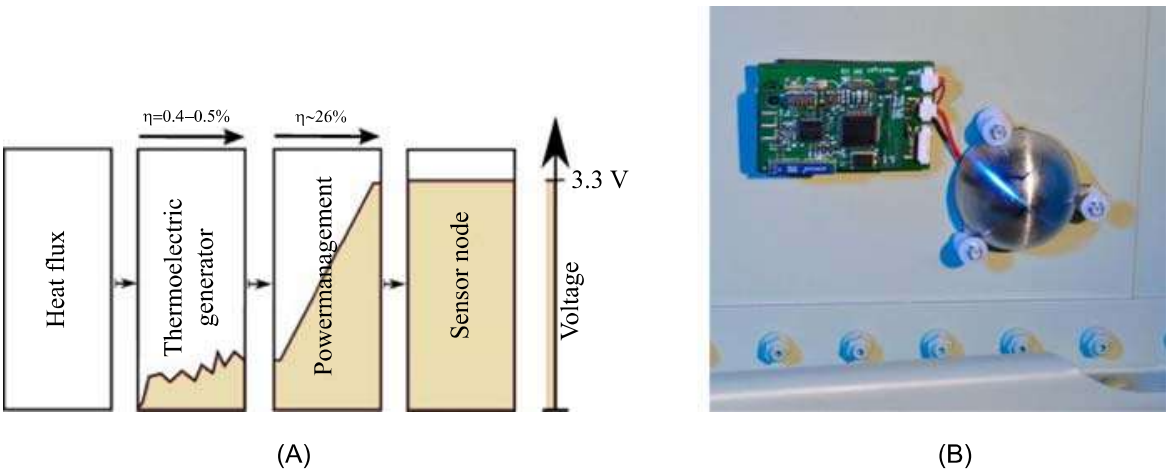

Figure 10.8 For the stand-alone prototype developed by Samson et al. and composed of the thermogenerator and the energy management chip (e.g., the MSP420 microcontroller) and the sensorial node (e.g., the crack sensor and the RF transceiver) [41]: (A) block diagram and (B) respective photo of a stand-alone prototype mounted on an aircraft hull for future tests. *Source*: Reproduced with the previous authorization of the publisher (*Elsevier*).

New innovative research was proposed by Ashby et al. [42], which proposes and claims (based on outstanding argumentation and supported by experimentation) a promising alternative to telluride-based materials (more specifically, with relation to the Bi_2Te_3), for example, materials based on silicon nanoparticles. In these materials, the thermal conductivity is low thanks to the high number of interfaces created [42]. Randomly distributed nanostructures in nanocomposite materials (see the concept in Fig. 10.9) can lead to a reduction in the thermal conductivity below that of an alloy of the same overall chemical stoichiometry [38,43]. This happens thanks to the high number of interfaces that are created, therefore increasing phonon scattering [42]. A thermoelectric figure-of-merit *ZT* of 0.6 at 300K was measured after subjecting silicon nanoparticles to a process of surface functionalization with phenylacetylene [42], whose value can be classified as significant (if not outstanding) for a bulk silicon.

10.2.2 Solar

One of the most important renewable energy sources is those based on photovoltaic (PV) cells [44–46] because their technology is well established in terms of maturity, applications, and markets. More recently, after the publication of the smart dust work [47], applications of solar photovoltaic to power stand-alone Microsystems started to know the interest for application on distributed sensors networks. In this classical work done by Warneke et al. [47] at the University of Berkley, a 16 mm^2-microsystem was fabricated for stand-alone operation through an integrated solar-cell. This microsystem was designed and fabricated to prove the concept in which it is possible to integrate three microdevices: (1) an SOI (Silicon-On-Insulator) solar cell to provide the power supply; (2) an ASIC fabricated on a 0.25 μm CMOS process, comprising a photosensor (a n-well/p-substrate CMOS photodiode), signal processing (amplification, analog-to-digital conversion) and control electronics (a state-machine with 13 states); and (3) by an optical transmitter [47]. The optical receiver was implemented within the CMOS ASIC through a second n-well/p-substrate photodiode because this is the CMOS photodetector configuration with the highest responsivity (e.g., highest sensitivity), while the optical

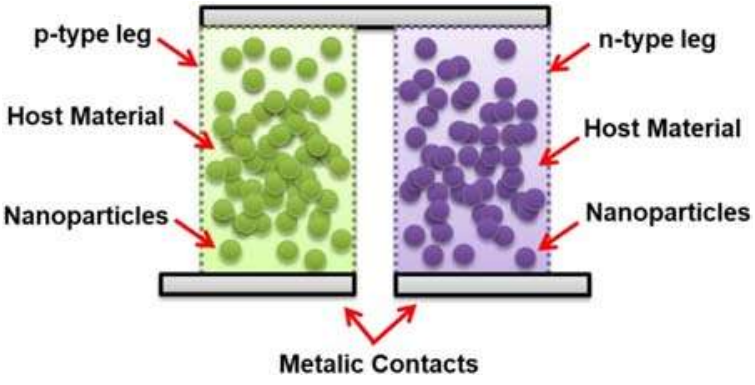

Figure 10.9 A thermocouple composed of a pair of n- and p-type legs, both made of nanocomposite materials.

transmitter was specifically implemented on a third microdevice composed of a micromachined four-quadrant corner-cube retroreflector (named as CCR chip) [47]. The optical transmission was made passive with respect to the target base-station to minimize the power consumption of the whole microsystem, for example, an interrogator in the base-station sends a light beam towards the microsystem in the direction of a set of 3 orthogonal mirrors. The bottom mirror is electrostatically actuated, thus the microsystem does nothing (saves power) for a "1" transmission. For a "0" transmission the bottom mirror is slightly actuated and displaced, breaking the orthogonality and thus spreading the light beam across the space [47]. This spreading is detected in the base-station because the received intensity is smaller for a "0" than for a "1." This ingenious solution results in a very low-power consumption microsystem.

Fig. 10.10 shows (A) the concept of an autonomous flexible thin-film (FTF) and (B)-(D) photos of an FTF functional prototype: (B) just after the application of polydimethylsiloxane (better known as PDMS), (C) after the PV cell placement, and (D) showing the maximum thickness of the FTF prototype [47]. Fig. 10.10A highlights the set of flexible substrates that compose the FTF, for example, a PV cell, a flexible PCB (fPCB), the PDMS material (a key-element between the three

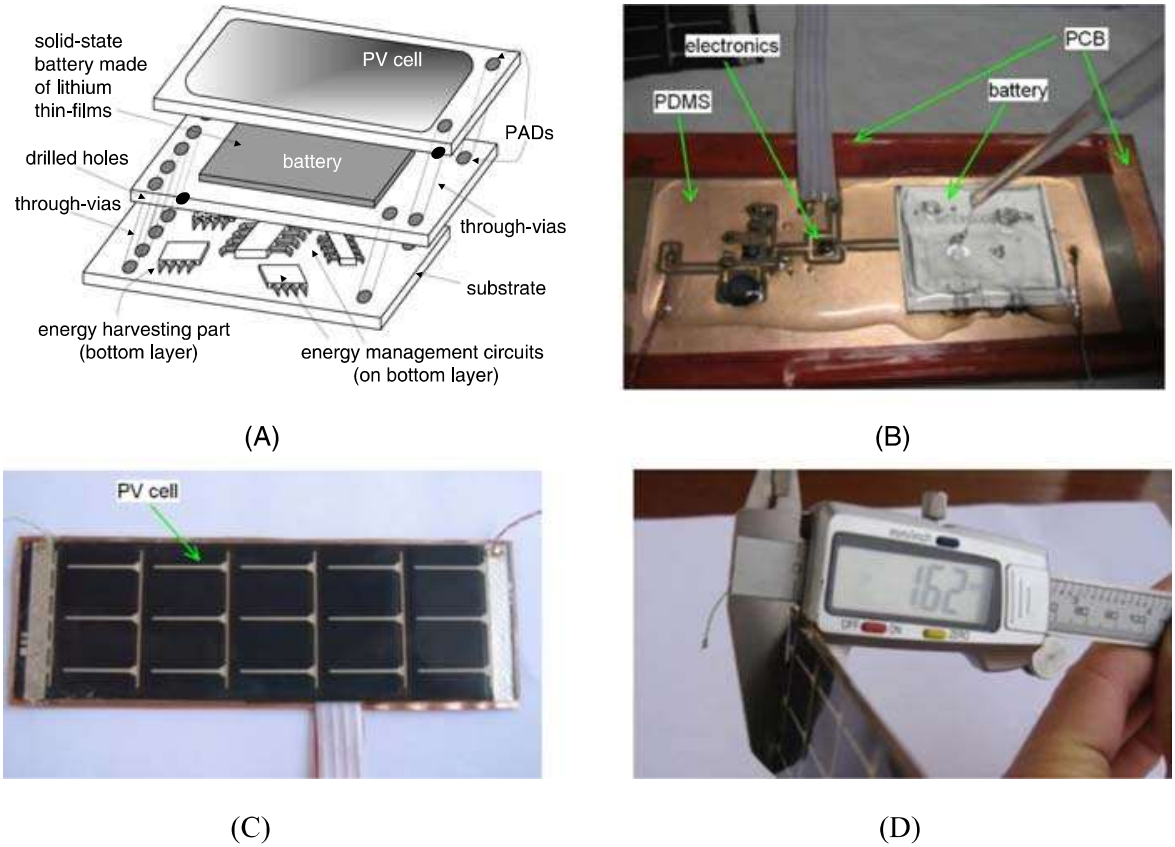

Figure 10.10 (A) Autonomous flexible thin-film (FTF) concept. Photos of the FTF prototype: (B) just after the PDMS application, (C) after the photovoltaic cell placement, and (D) showing the maximum thickness of the FTF [46].
Source: (B) and (C) were reproduced with the previous authorization of the publisher (*Elsevier*).

layers to serve as the adhesion layer) and the respective constructive concept. This FTF was designed and fabricated taking into account the growing need for deformable devices and transducers (either stretchable, foldable, or even compressible) [47–50]. The fPCB provides physical support to the electronics and battery, while the fPCB-PV cell adhesion is provided by a layer of PDMS. As shown in Fig. 10.10D, this TFT has a thickness of 1.62 mm, measures 37×114 mm^2, and weighs 10 g. This TFT was able to provide a voltage of 3.8 V under solar irradiations higher than 6 W m^{-2}, while values below the power were provided for the battery [47]. A certain degree of "intelligence" was thus required to make this energy management: a DC–DC step-up converter model LTC3105 incorporates an adjusted control for maximum power point tracking (MPPT) and was used to provide a regulated voltage for battery charging and power supply to the exterior. Additionally, it was necessary to either protect the battery from overvoltage peaks (during the charge) or undervoltage valleys (during the discharge). The LTC4071 was engaged to detect zones of danger and thus disconnect the battery from the charge/discharge circuit. The complete FTF schematic can be observed in Fig. 10.11.

This kind of energy harvester was designed and fabricated for applications where the need for maintenance should be reduced and solar energy is available and abundant. High-precision agriculture is a target field of applications matching these requirements [47–49].

A cutting-edge idea related to energy harvesting combines the physical characteristic to measure with the harvesting mechanism itself. This philosophy was followed by Emadi et al. [50] to design a self-powered Sun sensor to detect the satellite's position with respect to the Sun. The conventional approach shares with this one the use of 4 photodetectors on a matrix 2×2. Contrary to the former, the latter approach remains simple but ingenious because instead of a pin-hole aperture to allow only one photodetector to be illuminated when the array surface is aligned with the Sun, this last one takes into account the complementary situation [50]. In other words, only one photodetector is blocked and dark when the array is aligned

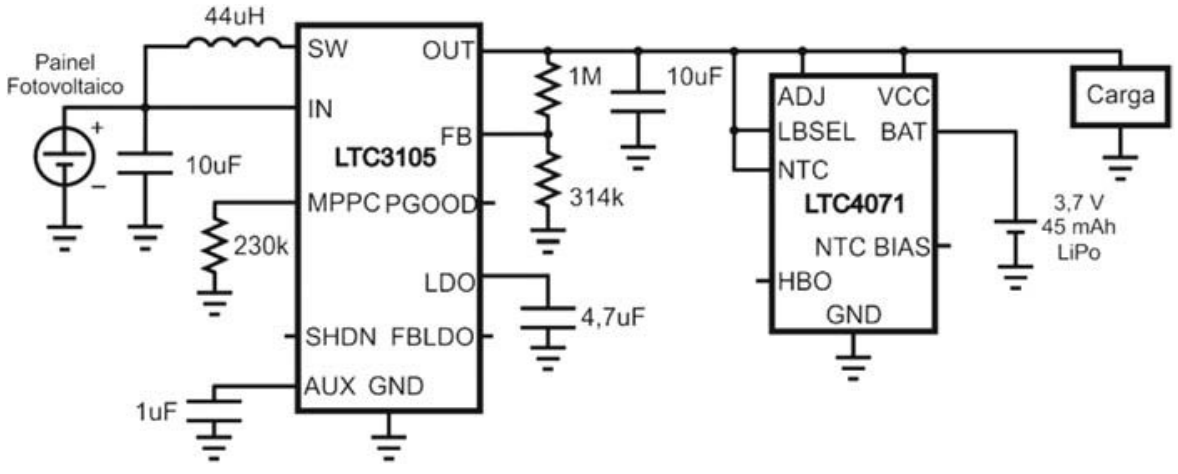

Figure 10.11 Electronic circuit composed of an maximum power point tracking step-up converter, a battery power management, and an under/over-voltage protection [46].

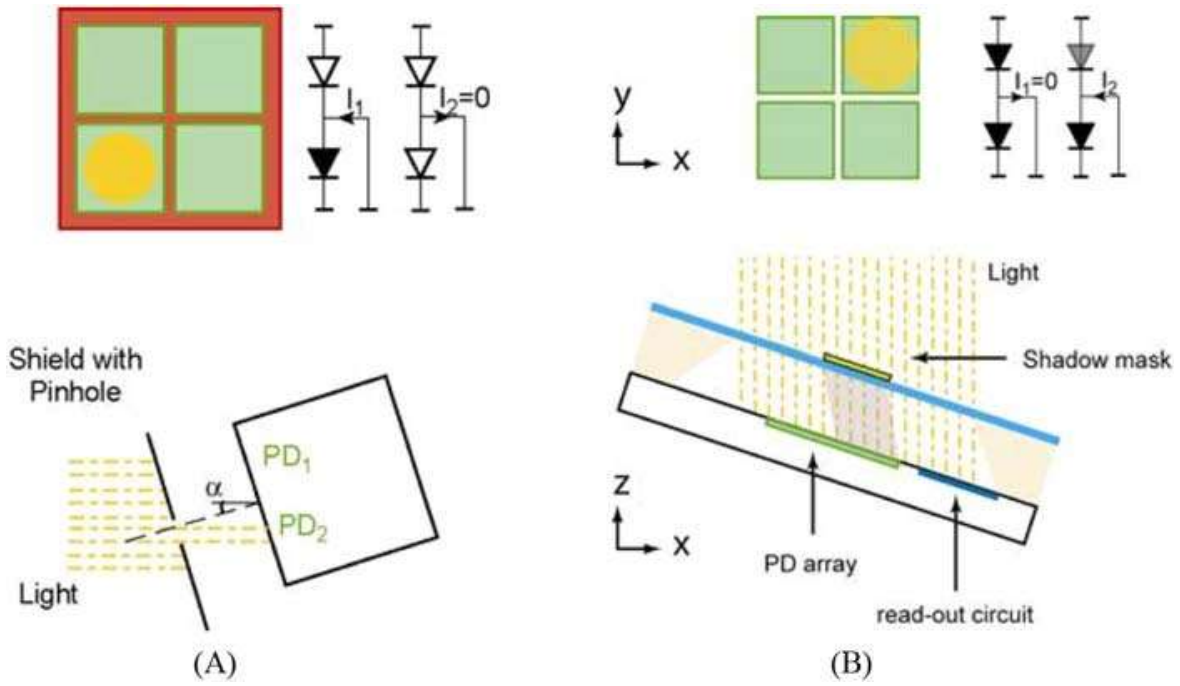

Figure 10.12 For the transduction on Sun sensors to align satellite panels: (A) conventional and (B) novel concepts [50].
Source: Reproduced with the previous authorization of the publisher (*Elsevier*).

with the Sun, allowing the collected photocurrents of the remaining 3 photodetectors to be used for both sensing and powering of the sensor. Fig. 10.12 illustrates the concept behind the (A) conventional and the (B) new approach [50].

Despite the abundant availability of solar light worldwide, this harvesting technique cannot be used in dark environments (oil wells, buried in the soil below the surface, embedded inside mechanical/physical structures, and so on). Another drawback related to this environmental power source is the lack of low-power/low-voltage solutions solar harvesting circuits observed at the industrial level, as concluded in a study conducted by Fröhlich et al. [51].

10.2.3 Piezoelectric

Piezoelectricity is the ability of a material to convert mechanical strain into electric current or voltage [52–55]. This effect is also reversible, by allowing the conversion of electricity into motion. While the first phenomenon is used on mechanical sensors and energy harvesters [56], the second phenomenon is used on mechanical actuators [57]. The most know class of applications is in footstep and footwear power generation [58,59]. Mechanical vibrations were proven to be one of the environmental energy sources with one of the highest delivered power and efficiency [60].

The most common materials used on both energy harvesting and mechanical actuation include: the lead-zirconate-titanate (PZT) [61], lead-titanate ($PbTiO_2$) [62], lead-zirconate ($PbZrO_3$) [63], barium-titanate ($BaTiO_3$) [64] and PVDF [65].

To date, the most used piezoelectric material is the PZT due to its inherent huge electromechanical coupling ability [66].

Despite the larger power handling, piezoelectric harvesting suffers from a huge drawback. As shown in Table 10.1, this kind of energy harvesting is strongly dependent on the natural frequency of oscillating, which is mainly imposed by the geometry of the movable part [67,68]. Behind the narrow-band feature, this poses a lot of problems concerned with miniaturization and integration in microsystems, for example, normally the resonance frequency increases with the object's size reduction [68]. Further improvements can be achieved by optimizing the shape of vibrational parts (for example, the shape of a cantilever and or a mass) [69]. However, nothing is more cutting-edge than the bimorph cantilever made of thick-films of PZT to explore the multimodality, allowing the piezoelectric converters to harvest energy from broadband vibrations [70].

The piezoelectricity is always surprising in the field of electronics. This can be confirmed through an emergent field in aeronautics, consisting of the electricity conversion from the aeroelastic vibration of the plane's wings [71–74]. Aeroelasticity is divided into static and dynamic aeroelastic phenomena. In the context of dynamic phenomena, it exists the flutter, which can present a high destructive potential. The flutter consists of self-sustained oscillations, happening on sustentation surfaces (e.g., on wings) when the flight speed is higher than a threshold (named critical speed of flutter). Below this threshold, the oscillations will be damped. A disturbance of any kind happening with flight speeds larger than the critical speed of flutter will result in auto-excited oscillations (e.g., like positive feedback in a physical system) with a fatal result for the sustaining structure. More recently and despite the potentially destructive nature of flutter, the recent research in aeronautics has confirmed its high potential to extract energy from the aeroelastic vibrations (resultant from the airflow) [72,75] to convert them into electrical energy for providing useful self-powered aeroelastic control methods [76]. In general terms, the idea is to harvest the energy on aeroelastic vibrations and use it to produce the same vibrations in the opposite direction. This implementation is no more than negative feedback towards the control of aeroelastic control.

10.2.4 Electronics and storage

A harvesting system composed only of the energy converter it is not enough to allow a microsystem to be fully stand-alone. Two additional energy processing stages comprising energy storage and power management are needed for a successful energy harvesting implementation [77,78]. In this context, the direct deposition of microbatteries into a microdevice (responsible for the energy management) was proposed by Lhermet et al. [79], making this work the first of this kind to be widely known in the literature. In Fig. 10.13 is possible to observe the block diagram of their microdevice/microbattery prototype [79], which forms a microsystem able to harvest (by transforming it into the electrical form) two power sources (e.g., inductive [80] and/or thermal [81]) and to manage the harvested energy through the microdevice. The microsystem is also able to store energy through microbattery.

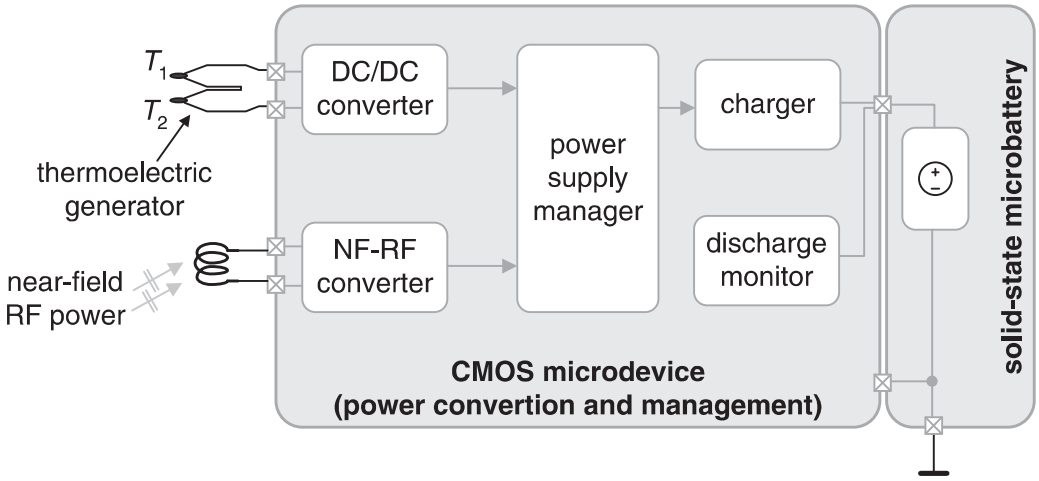

Figure 10.13 Block diagram of the microdevice/microbattery prototype fabricated by Lhermet et al. [79].

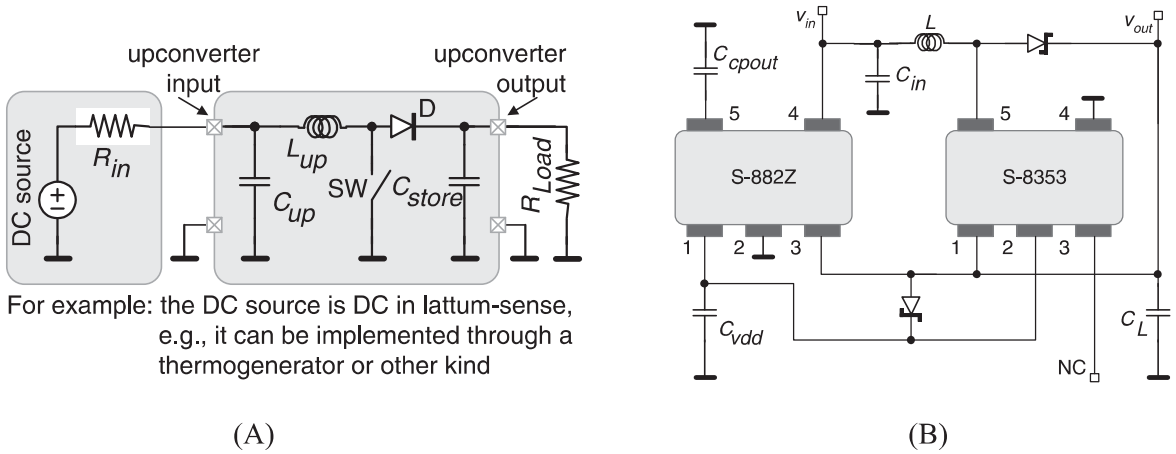

Figure 10.14 (A) Schematic of a simple voltage upconverter circuit. For the functional prototype of a voltage upconverter, using the Seikos' microdevices S-882Z and S-8353: (B) schematic.

In terms of power management, the microdevice can (1) schedule which external source will be used to charge the battery, even when both are available. The microsystem can also (2) provide a compatible voltage to the battery; make decisions about (3) stopping and (4) starting the charging process, as well as, (5) switch the provenience of power between the battery and the harvested source towards the load to supply it. This last control action allows the energy stored in the microbattery to be spared for situations when external power sources are not available.

After considering the specificities related to the energy type to be harvested, the block diagram of Fig. 10.13 can be considered a base for any power management circuit design. In this context and independently of the application, the DC/DC converter must be able to upconvert (or downconvert when necessary) the voltage from the external source. The voltage downconversion is straightforward to understand, thus, the focus will be placed on the upconversion. Fig. 10.14A illustrates a

schematic of a simple upconverter to help the physical principle behind this block [20]. An inductance L_{up} will be required to provide voltage peaking to achieve the upconversion, while a capacitor C_{up} [idealy] prevents the voltage to drop and thus, completing the upconversion process. In terms of operation, the current supplied by a DC source (for example, a thermogenerator) will charge C_{up}. Meanwhile, the switch SW closes and opens synchronously at a high frequency. When closed, the switch remains in this state for a short amount of time to reduce losses. This implies that, when closed, the signal responsible for commanding the switch must have a very low duty-cycle to avoid the capacitor C_{up} from over-discharge. The stored energy in the inductor L_{up} forces the capacitor C_{up} to discharge through the diode D, during the time the switch is opened (e.g., the diode makes a DC rectification). Finally, the current will charge the capacitor, C_{store}, which connects to the load (in the simplest configuration) or a DC regulator (on a more advanced configuration). The charge-capacity of C_{store} must be high to sustain [above a certain level] the voltage when deliver current to the load. This last configuration is very simple and easy to understand the principle behind the upconversion, using the step-up technique. On practical circuits, this configuration is very unsuitable due to the huge number of parameters to trade with the generator itself (switch on/off frequency, inductor L_{up}, capacitors C_{up}, and C_{store}, the forward voltage of diode D and the quality of electronic switch—for example, the open- and short-circuit losses within the switch). As illustrated in Fig. 10.14B, a more interesting solution can be implemented, using components off-the-shelf (COTS) [20]. Fig. 10.14B shows the electronic schematic of a circuit prototype for voltage upconversion through DC−DC step-upping, using the S-882Z (start-up microdevice for connecting into a step-up converter) and S-8353 (DC−DC step-up converter with PWM control and built-in switch) circuits from the Seiko manufacturer [82]. Table 10.2 shows few results for several sets of input voltages and currents, and as it can be observed the output voltage is very close to those required by a lithium battery ($\approx$3.7 V). A significant feature of the prototype based on these microdevices is their efficiency is always above 85%: Such efficiencies mean internal power losses below 15%, resulting in acceptable losses for these kinds of applications.

The combination of energy harvesting systems (comprising energy conversion and energy management systems) with batteries will expand and capability and autonomous features of stand-alone microsystems. However, this poses problems in terms of fully battery/microsystem integration because the battery technology didn't

Table 10.2 Few tests were made to the circuit of Fig. 10.14B−D for a few combinations of voltages and currents.

V_{in} [V]	I_{in} [ma]	V_{out} [V]	I_{out} [ma]	P_{in} [mW]	P_{out} [mW]	η [%]
0.31	40.11	3.20	3.32	12.43	10.62	85
0.39	45.30	3.40	5.05	17.57	17.17	98
0.45	50.50	3.60	5.91	22.70	20.68	91
0.50	70.10	4.50	7.55	35.05	33.97	97

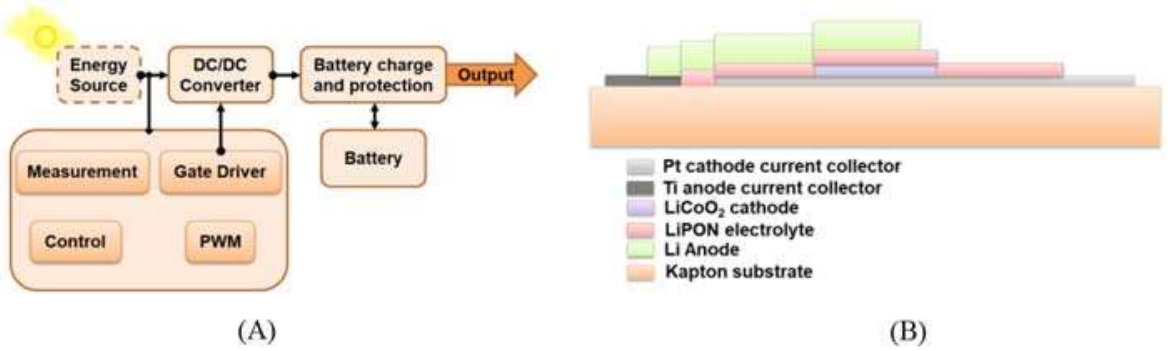

Figure 10.15 For solid-state microbattery made of thin-films fabricated by Ribeiro et al. [85]: (A) main blocks of a target application for this microbattery. (B) an artist's impression of the selected materials (not in the real scale for a better illustration).

follow the spectacular development of the microelectronics industry [83]. Nonetheless, this did not prevent the research and development of microbatteries for integration with microdevices as can be confirmed in Fig. 10.13 [79], illustrating the block diagram of the microdevice/microbattery prototype fabricated by Lhermet et al. [79]. Their microbattery was fabricated using microsystems techniques, more specifically the deposition of thin-films. The microbattery is of lithium type and was obtained through a stack of lithium/LiPON/TiSO, forming the cathode/electrolyte/anode respectively. More specific details about the fabrication of the microbattery can be found in their publications [78] and [84]. Ribeiro et al. [85] also have fabricated with success a solid-state microbattery on a flexible substrate made of polyimide (Kapton from DuPont). Fig. 10.15A illustrates the main blocks of a target application for this microbattery. The blocks of the energy harvesting system are comprised of a PV cell, which is intended to have a MPPT controller, a DC−DC converter, a battery charger and protection circuit and a microbattery itself. In this target application, the MPPT controller measures the voltage and current in the terminals of an energy source and calculates the necessary duty-cycle of the DC−DC converter. The battery charger and protection circuit control the flux of energy between the energy source, the battery, and the output of the energy harvesting system. The materials that compose the microbattery are a succession of layers made of $LiCoO_2$/LiPON/lithium that act as cathode/electrolyte/anode. In the future, a flexible solar cell is intended to be used as a substrate, where on its back side the microbattery was previously deposited using thin-film techniques by Ribeiro et al. elsewhere [85]. Further details about the deposition of the several materials that compose this battery can be found on [9,86].

10.3 Conclusions

This chapter has presented an overview of the state of the art related to energy harvesting systems for stand-alone microsystems (MSTs). It was intended to present hot-topics concerning this theme, especially those related to thermal, piezoelectric,

and solar photovoltaic. In the end, we presented a few integration topics concerning microelectronic systems and microbatteries for adding energy conversion/management and storage functions, respectively.

References

[1] B.R. Stojkoska, A.P. Avramova, P. Chatzimisios, Application of wireless sensor networks for indoor temperature regulation, Int. J. Distrib. Sens. Netw. 2014, 1−10. Paper #502419.

[2] Y. Cui, M. Kim, Y. Gu, J.-J. Jung, H. Lee, Home appliance management system for monitoring digitized devices using cloud computing technology in ubiquitous sensor network environment, Int. J. Distrib. Sens. Netw. 2014, 1−10, Paper #174097.

[3] T. Lu, X. Guo, Y. Li, Y. Peng, X. Zhang, F. Xie, et al., Cyberphysical security for industrial control systems based on wireless sensor networks, Int. J. Distrib. Sens. Netw. 2014 (2014) 1−17. Paper #438350.

[4] Z. Luo, P.S. Min, S.J. Liu, Target localization in wireless sensor networks for industrial control with selected sensors, Int. J. Distrib. Sens. Netw. 2013 (2013) 1−9. Paper #304631.

[5] K.-T. Yang, W.K. Lai, S.-M. Li, Y.-C. Lin, Event-based clustering architecture for power efficiency in wireless sensor networks, Int. J. Distrib. Sens. Netw. 2014, 1−12, Paper #612590.

[6] G. Yi, D. Yu, N. Kim, Adjusting control packet transmission intervals in low power sensor systems, Int. J. Distrib. Sens. Netw. 2014, 1−8, Paper #139682.

[7] Y. Cui, M. Kim, Y. Gu, J.-J. Jung, H. Lee, Home appliance management system for monitoring digitized devices using cloud computing technology in ubiquitous sensor network environment, Int. J. Distrib. Sens. Netw. 2014, 1−10, Paper #174097.

[8] K.H. Park, A ubiquitous motion tracking system using sensors in a personal health device, Int. J. Distrib. Sens. Netw. 2013 (2013) 1−6. Paper #298209.

[9] S. Akbari, Energy harvesting for wireless sensor networks review, in: Proceeding of the 2014 Federated Conference on Computer Science and Information Systems, vol. 2, Warsaw, 2014, pp. 987−992.

[10] L. Mateu, C. Codrea, N. Lucas, M. Pollak, P. Spies, Human body energy harvesting thermogenerator for sensing applications, in: Proceeding of the 2007 International Conference na Sensor Technologies and Applications, Valencia, Spain, October 2007, pp. 366 272.

[11] L. Collins, Harvest for the world, IEEE Power Eng. J. 20 (1) (2006) 34−37.

[12] J. Bouchaud, R. Dixon, Micro-energy harvesters: overview, applications and markets, in: MSTnews: International Newsletter on Micro Nano Integration, No. 1l08, February 2008, pp. 18 19.

[13] D. Dondi, A. Bertacchini, D. Brunelli, L. Larcher, L. Benini, Modeling and optimization of a solar energy harvester system for self-powered wireless sensor networks, IEEE Trans. Ind. Electron. 55 (7) (2008) 2759−2766.

[14] L. Mateu, F. Moll, Appropriate charge control of the storage capacitor in a piezoelectric energy harvesting device for discontinuous load operation, J. Sens. Actuators A: Phys. Sens. 132 (2006) 302−310.

[15] J. Liu, J. Yao, Wireless RF identification system based on SAW, IEEE Trans. Ind. Electron. 55 (2) (2008) 958−961.

[16] L. Bell, Cooling, heating, generating power, and recovering waste heat with thermoelectric systems, Science 321 (2008) 1457–1461.
[17] B. Poudel, Q. Hao, Y. Ma, Y. Lan, A. Minnich, B. Yu, et al., High-thermoelectric performance of nanostructured bismith antomony telluride bulk alloys, Science 320 (2008) 634–637.
[18] M.S. Dresselhaus, G. Chen, M.Y. Tang, R. Yang, H. Lee, D. Wang, et al., New directions for low-dimensional thermoelectric materials, Adv. Mater. 19 (2007) 1–12.
[19] A. Böttner, G. Chen, R. Venkatasubramanian, Aspects of thin-film superlattice thermoelectric materials, devices, and applications, MRS Bull. 31 (2006) 211–217.
[20] J.P. Carmo, L.M. Goncalves, J.H. Correia, Thermoelectric microconverter for energy harvesting systems, IEEE Trans. Ind. Electron. 57 (2010) 861–867.
[21] J.P. Carmo, J. Antunes, M.F. Silva, J.F. Ribeiro, L.M. Goncalves, J.H. Correia, Characterization of thermoelectric generators by measuring the load-dependence behavior, Measurement 44 (2011) 2194–2199.
[22] J.P. Carmo, L.M. Goncalves, R.F. Wolffenbuttel, J.H. Correia, A planar thermoelectric power generator for integration in wearable microsystems, Sens. Actuators A 161 (2010) 199–204.
[23] S.M. Yang, T. Lee, C.A. Jeng, Development of a thermoelectric energy harvester with thermal isolation cavity by standard CMOS process, Sens. Actuators A 153 (2009) 244–250.
[24] R. Carta, P. Jourand, B. Hermans, J. Thoné, D. Brosteaux, T. Vervust, et al., Design and implementation of advanced systems in a flexible-stretchable technology for biomedical applications, Sens. Actuators A 156 (2009) 79–87.
[25] N.S. Dias, J.P. Carmo, P.M. Mendes, J.H. Correia, A low power/low voltage CMOS wireless interface at 5.7 GHz with dry electrodes for cognitive networks, IEEE Sens. J. 11 (2011) 755–762.
[26] N.S. Dias, J.P. Carmo, P.M. Mendes, J.H. Correia, Wireless instrumentation system based on dry electrodes for acquiring EEG signals, Med. Eng. Phys. 43 (2012) 972–978.
[27] M.S. Fernandes, J.H. Correia, P.M. Mendes, Electro-optic acquisition system for ECG wearable sensor applications, Sens. Actuators A 203 (2013) 316–323.
[28] P. Zhao, N. Deng, X. Li, C. Ren, Z. Wang, Development of highly-sensitive and ultra-thin silicon stress sensor chips for wearable biomedical applications, Sens. Actuators A 216 (2014) 158–166.
[29] Y.D. Lee, W.Y. Chung, Wireless sensor network based wearable smart shirt for ubiquitous health and activity monitoring, Sens. Actuators B 140 (2009) 390–395.
[30] M. Ozawaa, K. Sampeia, C. Cortesa, M. Ogawaa, A. Oikawaa, N. Miki, Wearable line-of-sight detection system using micro-fabricated transparent optical sensors on eyeglasse, Sens. Actuators A 205, 208 214, 1014.
[31] R.F. Yazicioglu, T. Torfs, P. Merken, J. Penders, V. Leonov, R. Puers, et al., Ultra-low-power biopotential interfaces and their applications in wearable and implantable systems, Microelectron. J. 40 (2009) 1313–1321.
[32] Body Area Networks, IMEC's 2012 activity report. [online] http://annualreport.imec.be/Domains/page.aspx/1203.
[33] R. Carta, M. Sfakiotakis, N. Pateromichelakis, J. Thoné, D.P. Tsakiris, R. Puers, A multi-coil inductive powering system for an endoscopic capsule with vibratory actuation, Sens. Actuators A 172 (2011) 253–258.
[34] Z. Wang, V. Leonov, P. Fiorini, C.V. Hoof, Realization of a wearable miniaturized thermoelectric generator for human body applications, Sens. Actuators A 156 (2009) 95–102.

[35] M. Takashiri, T. Shirakawa, K. Miyazaki, H. Tsukamoto, Fabrication and characterization of bismuth-telluride-based alloy thin film thermoelectric generators by flash evaporation method, Sens. Actuators A 138 (2007) 329–334.
[36] L.M. Gonçalves, C. Couto, P. Alpuim, A.G. Rolo, F. Völklein, J.H. Correia, Optimization of thermoelectric properties on Bi_2Te_3 thin films deposited by thermal co-evaporation, Thin Solid. Films 518 (2010) 2816–2821.
[37] L.M. Goncalves, P. Alpuim, A.G. Rolo, J.H. Correia, Thermal co-evaporation of Sb_2Te_3 thin-films optimized for thermoelectric applications, Thin Solid. Films 519 (2011) 4152–4157.
[38] M.F. Silva, J.F. Ribeiro, J.P. Carmo, L.M. Gonçalves, J.H. Correia, Thin-films for thermoelectric applicationsISBN: 978-3-642-25413-0 in: B. Bhushan (Ed.), Invited Book Chapter in the book Scanning Probe Microscopy in Nanoscience and Nanotechnology 3, Springer, 2012.
[39] J. Weber, K. Potje-Kamloth, F. Haase, P. Detemple, F. Völklein, T. Doll, Coin-size coiled-up polymer foil thermoelectric power generator for wearable electronics, Sens. Actuators A 132 (2006) 325–330.
[40] N. Wojtas, E. Schwytera, W. Glatz, S. Kühne, W. Escher, C. Hierold, Power enhancement of micro thermoelectric generators by microfluidic heat transfer packaging, Sens. Actuators A 188 (2012) 389–395.
[41] D. Samson, M. Kluge, T. Becker, U. Schmid, Wireless sensor node powered by aircraft specific thermoelectric energy harvesting, Sens. Actuators A 172 (2011) 240–244.
[42] S. Ashby, J.A. Thomas, J. García Cañadas, G. Min, J. Corps, A.V. Powell, et al., FD 176: Bridging silicon nanoparticles and thermoelectrics: phenylacetylene functionalization, in: Faraday Discussions, Accepted for publication on 26th June 2014. Available from: https://doi.org/10.1039/C4FD00109E.
[43] L.M. Gonçalves, Thermoelectric Microsystem Based on Bismuth and Antimony Tellurides (PhD thesis), University of Minho, 2008.
[44] R. Eke, A.S. Kavasoglu, N. Kavasoglu, Design and implementation of a low-cost multi-channel temperature measurement system for photovoltaic modules, Measurement 45 (2012) 1499–1509.
[45] M. Gagliarducci, D.A. Lampasi, L. Podestà, GSM-based monitoring and control of photovoltaic power generation, Measurement 40 (2007) 314–321.
[46] J.P. Carmo, J.M. Gomes, L.M. Gonçalves, J.H. Correia, A flexible thin-film for powering stand-alone electronic devices, Measurement 46 (10) (2013) 4145–4151.
[47] B. Warneke, M. Scott, B. Leibowitz, Z. Lixia, C. Bellew, J. Chediakl, et al., An autonomous 16 mm^3 solar-powered node for distributed wireless sensor networks, in: Proceedings of the IEEE Sensors, vol. 2, June 2002, pp. 1510 1515.
[48] R. Morais, M.A. Fernandes, S.G. Matos, C. Serôdio, P.J.S.G. Ferreira, M.J.C.S. Reis, A ZigBee multi-powered wireless acquisition device for remote sensing applications in precision viticulture, Comput. Electron. Agric. 62 (2008) 94–106.
[49] R. Morais, S.G. Matos, M.A. Fernandes, A.L.G. Valente, S.F.S.P. Soares, P.J.S.G. Ferreira, et al., Sun, wind and water flow as energy supply for small stationary data acquisition platforms, Comput. Electron. Agric. 64 (2008) 120–132.
[50] H. Wu, A. Emadi, G. de Graaf, J. Leijtens, R.F. Wolffenbuttel, Self-powered sun sensor microsystems, Procedia Chem. 1 (2009) 1363–1366.
[51] A.A. Frolich, E.A. Bezerra, L.K. Slongo, Experimental analysis of solar energy harvesting circuits efficiency for low power applications, in: Computers and Electrical Engineering, Accepted for publication on 5th October 2014. Available from: https://doi.org/10.1016/j.compeleceng.2014.09.004.

[52] R. Caliò, U.B. Rongala, D. Camboni, M. Milazzo, C. Stefanini, G. de Petris, et al., Piezoelectric energy harvesting solutions, Sensors 14 (2014) 4755–4790.
[53] A. Venugopal, A. Agrawal, S.V. Prabhu, Performance evaluation of piezoelectric and differential pressure sensor for vortex flowmeters, Measurement 50 (2014) 10–18.
[54] I. Korhonen, R. Lankinen, Energy harvester for a wireless sensor in a boiler environment, Measurement 58 (2014) 241–248.
[55] B.V.M.P.S. Kumar, K. Suresh, U.V. Kumar, G. Uma, M. Umapathy, Resonance based DC current sensor, Measurement 45 (2012) 369–374.
[56] A. Bounouh, D. Bélières, Resonant frequency characterization of MEMS based energy harvesters by harmonic sampling analysis method, Measurement 52 (2014) 71–76.
[57] M.L. Jansen, G.R. Willmott, I. Hoek, W.M. Arnold, Fast piezoelectric actuation of an elastomeric micropore, Measurement 46 (2013) 3560–3567.
[58] J.G. Rocha, L.M. Gonçalves, P.F. Rocha, M.P. Silva, S. Lanceros-Méndez, Energy harvesting from piezoelectric materials fully integrated in footwear, IEEE Trans. Ind. Electron. 57 (2010).
[59] L. Xie, M. Cai, Increased piezoelectric energy harvesting from human footstep motion by using an amplification mechanism, Appl. Phys. Lett. 105 (2014) 1–4. Paper #143901.
[60] P.C.-P. Chao, Energy harvesting electronics for vibratory devices in self-powered sensors, IEEE Sens. J. 11 (2011) 3106–3121.
[61] R. Medeiros, M.L. Ribeiro, M. Sartorato, G. Marinucci, V. Tita, Computational simulation using PZT as sensor elements for damage detection on impacted composite cylinders, in: Proceedong of the 1st International Symposium on Solid Mechanics (MecSol2013), Porto Alegre, Rio Grande do Sul RS, Brazil, 2013, pp. 1–11.
[62] G.R. Blake, A.R. Armstrong, E. Sastre, W. Zhou, P.A. Wright, The preparation of a novel layered lead titanate and its conversion to the perovskite lead titanate $PbTiO_3$, Mater. Res. Bull. 36 (2001) 1837–1845.
[63] A. Kimoto, J.D. Maddumapatabendi, A proposal of multi-imaging system of electrical and ultrasonic properties, Measurement 44 (2011) 2000–2007.
[64] A. Stashans, H. Pinto, Analysis of radiation-induced hole localisation in titanates, Radiat. Meas. 33 (2001) 553–555.
[65] D. Chen, T. Sharma, J.X.J. Zhang, Mesoporous surface control of PVDF thin films for enhanced piezoelectric energy generation, Sens. Actuators A 216 (2014) 196–201.
[66] A. Nechibvute, A. Chawanda, P. Luhanga, Piezoelectric energy harvesting devices: an alternative energy source for wireless sensor, Smart Mater. Res. 2012, 1–13, Paper #853481.
[67] A. Tabesh, L.G. Frechette, A low-power stand-alone adaptive circuit for harvesting energy from a piezoelectric micropower generator, IEEE Trans. Ind. Electron. 57 (2010) 840–849.
[68] A. Khaligh, P. Zeng, C. Zheng, Kinetic energy harvesting using piezoelectric and electromagnetic technologies state of the art, IEEE Trans. Ind. Electron. 57 (2010) 850–860.
[69] W.G. Li, S. He, S. Yu, Improving power density of a cantilever piezoelectric power harvester through a curved L-shaped proof mass, IEEE Trans. Ind. Electron. 57 (2011) 868–876.
[70] M. Baù, M. Ferrari, E. Tonoli, V. Ferrari, Sensors and energy harvesters based on piezoelectric thick films, Procedia Eng. 25 (2011) 737–744.
[71] M. Rosa, C. De Marqui Junior, Modeling and analysis of a piezoelectric energy harvester with varying cross-sectional area, Shock. Vib. 2014 1–9. Paper #930503.

[72] J.A.C. Dias, C. De Marqui Junior, A. Erturk, Hybrid piezoelectric-inductive flow energy harvesting and dimensionless electroaeroelastic analysis for scaling, Appl. Phys. Lett. 102 (2013) 1–5. paper #044101.
[73] C. De Marqui Junior, A. Erturk, Electroaeroelastic analysis of airfoilbased wind energy harvesting using piezoelectric transduction and electromagnetic induction, J. Intell. Mater. Syst. Struct. 24 (2013) 846–854.
[74] A.J. Dias, C. De Marqui Junior, A. Erturk, Three-degree-of-freedom hybrid piezoelectric-inductive aeroelastic energy harvester exploiting a control surface, Am. Inst. Aeronautics Astronautics J. (2014) 1–11.
[75] M. Bryant, E. Wolff, E. Garcia, Aeroelastic flutter energy harvester design: the sensitivity of the driving instability to system parameters, Smart Mater. Struct. 20 (2011) 1–12.
[76] D. D'Assunção, C. De Marqui Junior, Applied self-powered semi-passive control for a 2-degree-of-freedom aeroelastic typical section using shunted piezoelectric materials, J. Intell. Mater. Syst. Struct. (2014) 1–13. Available from: https://doi.org/10.1177/1045389X14526797.
[77] J.P. Carmo, J.F. Ribeiro, M.F. Silva, L.M. Goncalves, J.H. Correia, Thermoelectric generator and solid-state battery for stand-alone microsystems, J. Micromech. Microeng. 20 (2010) 1–8.
[78] R. Salot, S. Bancel, S. Martin, G. Savelli, C. Salvi, M. Plissonnier, Thermoelectric and microbattery hybrid system with its power management, in: Proceeding of the Symposium Design Test Integration & Packaging of MEMS/MOEMS 349 353, 2006.
[79] H. Lhermet, C. Condemine, M. Plissonnier, R. Salot, P. Audebert, M. Rosset, Efficient power management circuit: from thermal energy harvesting to above IC microbattery energy storage, IEEE J. Solid. State Circuits 43 (2008) 246–255.
[80] H. Lhermet, C. Condemine, R. Salot, M. Plissonnier, S. Bacquet, P. Audebert, On chip post processed microbattery powered with RF and thermal energy through a power management circuit, in: Proceeding of the IEEE International Conference on Integrated Circuit Design an Technology, 2007, pp. 184–186.
[81] G. Savelli, M. Plissonnier, J. Bablet, C. Salvi, J.M. Fournier, Energy conversion using new thermoelectric generator, in: Proceeding of the Symposium Design Test Integration & Packaging of MEMS/MOEMS, 2006, pp. 369–374.
[82] Seiko Instruments Inc. [online]. http://www.sii-ic.com/en/semicon/.
[83] M. Armand, J.M. Tarascon, Building better batteries, Nature 451 (2008) 652–657.
[84] S. Oukassi, X. Gagnard, R. Salot, S. Bancel, J.P. Pereira Ramos, Above IC micro power generators for RF MEMS, in: Proceeding of the Symposium Design Test Integration & Packaging of MEMS/MOEMS, 2006, pp. 1–4.
[85] J.F. Ribeiro, R. Sousa, J.A. Sousa, L.M. Goncalves, M.M. Silva, L. Dupont, et al., Flexible thin-film rechargeable lithium batteries, in: Proceeding of the Transducers 2013, Barcelona, Spain, 2013.
[86] J.F. Ribeiro, R. Sousa, J.P. Carmo, L.M. Gonçalves, M.F. Silva, M.M. Silva, et al., Enhanced solid-state electrolytes made of lithium phosphorous oxynitride films, Thin Solid. Films 552 (2012) 85–89.